



**QUEEN'S
UNIVERSITY
BELFAST**

Oscillatory Dynamics of Perceptual to Conceptual Transformations in the Ventral Visual Pathway

Clarke, A., Devereux, B. J., & Tyler, L. K. (2018). Oscillatory Dynamics of Perceptual to Conceptual Transformations in the Ventral Visual Pathway. *Journal of cognitive neuroscience*, 30(11), 1590-1605.
https://doi.org/10.1162/jocn_a_01325

Published in:
Journal of cognitive neuroscience

Document Version:
Publisher's PDF, also known as Version of record

Queen's University Belfast - Research Portal:
[Link to publication record in Queen's University Belfast Research Portal](#)

Publisher rights
© 2018 Massachusetts Institute of Technology.
This work is made available online in accordance with the publisher's policies. Please refer to any applicable terms of use of the publisher.

General rights
Copyright for the publications made accessible via the Queen's University Belfast Research Portal is retained by the author(s) and / or other copyright owners and it is a condition of accessing these publications that users recognise and abide by the legal requirements associated with these rights.

Take down policy
The Research Portal is Queen's institutional repository that provides access to Queen's research output. Every effort has been made to ensure that content in the Research Portal does not infringe any person's rights, or applicable UK laws. If you discover content in the Research Portal that you believe breaches copyright or violates any law, please contact openaccess@qub.ac.uk.

Oscillatory Dynamics of Perceptual to Conceptual Transformations in the Ventral Visual Pathway

Alex Clarke^{1,2}, Barry J. Devereux^{1,3}, and Lorraine K. Tyler¹

Abstract

■ Object recognition requires dynamic transformations of low-level visual inputs to complex semantic representations. Although this process depends on the ventral visual pathway, we lack an incremental account from low-level inputs to semantic representations and the mechanistic details of these dynamics. Here we combine computational models of vision with semantics and test the output of the incremental model against patterns of neural oscillations recorded with magnetoencephalography in humans. Representational similarity analysis showed visual information was represented in low-frequency

activity throughout the ventral visual pathway, and semantic information was represented in theta activity. Furthermore, directed connectivity showed visual information travels through feedforward connections, whereas visual information is transformed into semantic representations through feedforward and feedback activity, centered on the anterior temporal lobe. Our research highlights that the complex transformations between visual and semantic information is driven by feedforward and recurrent dynamics resulting in object-specific semantics. ■

INTRODUCTION

Visual object recognition requires dynamic transformations of information from low-level visual inputs to higher-level visual properties and ultimately complex semantic representations. These processes rely on the ventral visual pathway (VVP) from the occipital lobe along the ventral surface of the temporal lobe (Kravitz, Saleem, Baker, Ungerleider, & Mishkin, 2013), with the perirhinal cortex (PRC) sitting at the apex of the pathway (Clarke & Tyler, 2014; Tyler et al., 2013; Barense et al., 2012; Cowell, Bussey, & Saksida, 2010; Taylor, Moss, Stamatakis, & Tyler, 2006; Bussey & Saksida, 2002). Along the VVP, object representations become increasingly complex and abstracted from their inputs, such that higher-level visual properties are coded in lateral occipital cortex (LOC) and posterior inferior temporal cortex (IT) that show object invariance (Kravitz et al., 2013; DiCarlo, Zoccolan, & Rust, 2012), alongside conceptual properties of objects that are sufficient to distinguish between different superordinate categories (Tyler et al., 2013). In contrast, object-specific semantic representations are seen in the PRC, at the most anterior part of the VVP, which is hypothesized to form complex conjunctions of properties from more posterior regions to enable fine-grained distinctions between conceptually similar objects

(Clarke & Tyler, 2014; Tyler et al., 2004, 2013; Barense et al., 2012; Kivisaari, Tyler, Monsch, & Taylor, 2012; Cowell et al., 2010; Bussey & Saksida, 2002). Yet this view of recognition—where both activity and the complexity of object information progresses along the posterior to anterior axis in the VVP—is fundamentally incomplete as it does not take into account the temporal dynamics of feedforward and feedback processes and their interactions.

The brain's anatomical structure suggests that complex interactions between bottom-up and top-down processes must be a key part of object processing, as demonstrated by the abundance of lateral and feedback anatomical connections within the VVP and beyond (Bullier, 2001; Lamme & Roelfsema, 2000). Research using time-resolved imaging methods have shown that both feedforward and recurrent dynamics in the VVP underpin object representations, where visual inputs activate semantic information within the first 150 msec and object-specific semantic representations emerge beyond 200 msec supported by recurrent activity between the anterior temporal lobe (ATL) and the posterior VVP (Clarke, Devereux, Randall, & Tyler, 2015; Poch et al., 2015; Clarke, Taylor, Devereux, Randall, & Tyler, 2013; Chan et al., 2011; Clarke, Taylor, & Tyler, 2011; Schendan & Maher, 2009).

Although this research provides spatial and temporal signatures of the fundamental aspects of recognition—namely visual and semantic processing—two important limitations remain. First, research tends to focus on three aspects of objects—low-level visual properties, superordinate category information (e.g., animals, tools, animate/inanimate), and object-specific semantics (e.g., tiger, hammer). This paints a compartmentalized picture that

This paper is part of a Special Focus deriving from a symposium at the 2017 annual meeting of Cognitive Neuroscience Society, entitled, “The Dynamics of Cognitive Processes: Multivariate Approaches.”

¹University of Cambridge, ²Anglia Ruskin University, Cambridge, United Kingdom, ³Queen's University Belfast

fails to capture the incremental transitions whereby vision seamlessly activates meaning. Second, although there is increasing knowledge of the oscillatory mechanisms underpinning basic visual processing (Jensen, Gips, Bergmann, & Bonnefond, 2014; Tallon-Baudry & Bertrand, 1999), models of how visual inputs activate meaning lack such detail. Here, we overcome these limitations by combining current computational models of vision with a model of semantics to obtain quantifiable estimates of the incremental representations from low-level visual inputs to complex semantic representations. This model is then tested against neural activity using representational similarity analysis (RSA; Nili et al., 2014; Kriegeskorte, Mur, & Bandettini, 2008) to reveal how oscillatory activity along the VVP codes for visual and semantic object properties.

Deep neural networks (DNNs) have proved highly successful for vision, both to provide an engineering solution to labeling objects (Krizhevsky, Sutskever, & Hinton, 2012) and to map the outputs from the DNN to brain representations of objects in space and time (Devereux, Clarke, & Tyler, 2018; Seeliger et al., 2017; Cichy, Khosla, Pantazis, Torralba, & Oliva, 2016; Güçlü & van Gerven, 2015; Cichy, Pantazis, & Oliva, 2014). DNNs for vision are composed of multiple layers, and as the layers progress, the nodes become sensitive to more complex, higher-level visual image features in a similar progression to the human VVP (Devereux et al., 2018; Cichy et al., 2014, 2016; Güçlü & van Gerven, 2015). However, current DNNs tell us little about an object's semantic representation. Although visual DNNs can provide accurate labels for images, the output layers do not capture how different objects are related in meaning. This is revealed by recent fMRI research, showing that, although DNNs explain visual processes in the posterior ventral temporal cortex (pVTC), additional semantic computational models are required to capture the semantic information about object representations in the pVTC and the PRC (Devereux et al., 2018). This work used a recurrent attractor network (AN) for object semantics, as ANs have been shown to capture how objects semantically relate to one another (Devereux, Taylor, Randall, Geertzen, & Tyler, 2016; Cree, McNorgan, & McRae, 2006; Cree, McRae, & McNorgan, 1999). This occurs because the activation across the nodes in the model captures the activation of different semantic features (such as "is round," "has a handle," "is thrown," etc.). Furthermore, the dynamics of how these nodes become activated mirrors both behavioral responses and magnetoencephalography (MEG) time courses during object recognition (Devereux et al., 2016; Clarke et al., 2013; Randall, Moss, Rodd, Greer, & Tyler, 2004). Together, the DNN and AN provide complementary aspects of object recognition. As in Devereux et al. (2018), by using the output of the visual DNN as input into the semantic AN, we further provide a potential route by which visual representations can directly activate semantic knowledge. Most importantly, however, combining the DNN and AN gives us a quantifiable computational

approach that models the incremental visual and semantic properties of objects, from low-level vision to high-level semantics. This approach can be combined with RSA for dynamic measures of brain activity to show how different types of visual and semantic information are coded in dynamic patterns of brain activity along the VVP.

The brain activities we focus on here are neural oscillations. Oscillations are a ubiquitous property of the brain and are known to be modulated by various aspects of vision and memory in humans (Helfrich & Knight, 2016; Watrous, Fell, Ekstrom, & Axmacher, 2015; Jensen et al., 2014; Hanslmayr, Staudigl, & Fellner, 2012; Fell & Axmacher, 2011). Recent studies have begun to show how the ongoing phase of an oscillation can be used to decode specific stimuli (Michelmann, Bowman, & Hanslmayr, 2016; Staudigl, Vollmar, Noachtar, & Hanslmayr, 2015; Watrous, Deuker, Fell, & Axmacher, 2015; Lopour, Tavassoli, Fried, & Ringach, 2013; Ng, Logothetis, & Kayser, 2013; Kayser, Ince, & Panzeri, 2012; Turesson, Logothetis, & Hoffman, 2012; Schyns, Thut, & Gross, 2011; Montemurro, Rasch, Murayama, Logothetis, & Panzeri, 2008). These studies have shown that frequency-specific activity can be used to decode the specific features of visual objects or object categories, suggesting that the oscillatory phase could provide a mechanism for encoding stimulus information within a region. Furthermore, oscillations may help to coordinate the activity between regions in the VVP, enabling object information to be transformed over space and time as meaning is accessed from vision.

Here, we combine RSA with neural oscillations and computational models that could provide an important advance in determining the dynamic flow of different types of object information during recognition—both in terms of how different regions represent visual and semantic information and how information is transformed across regions. To achieve this, we recorded MEG while participants viewed a large set of common objects from diverse superordinate categories. The combined DNN and AN models provided predictions for how objects should be similar to one another, and these predictions were tested against the MEG data using RSA (Figure 1). The MEG signals were source-localized, and single-object oscillatory phase patterns were extracted from five ROIs in the VVP. Based on these phase patterns across objects, we could determine how similar objects were to each other within each ROI and track this over time and frequency. RSA then allows us to test the degree to which the object similarity, according to the computational model, is reflected in oscillatory phase signals over space, time, and frequency. We predict both a spatial and temporal hierarchy in the VVP between visual object information and semantics. Crucially, recurrent activity will be associated with the activation of semantic object information that will also depend on the coordinated activity within the VVP. Although visual object properties are predicted in theta and alpha (VanRullen, Zoefel, & Ilhan, 2014; Kayser et al., 2012; Montemurro et al., 2008),

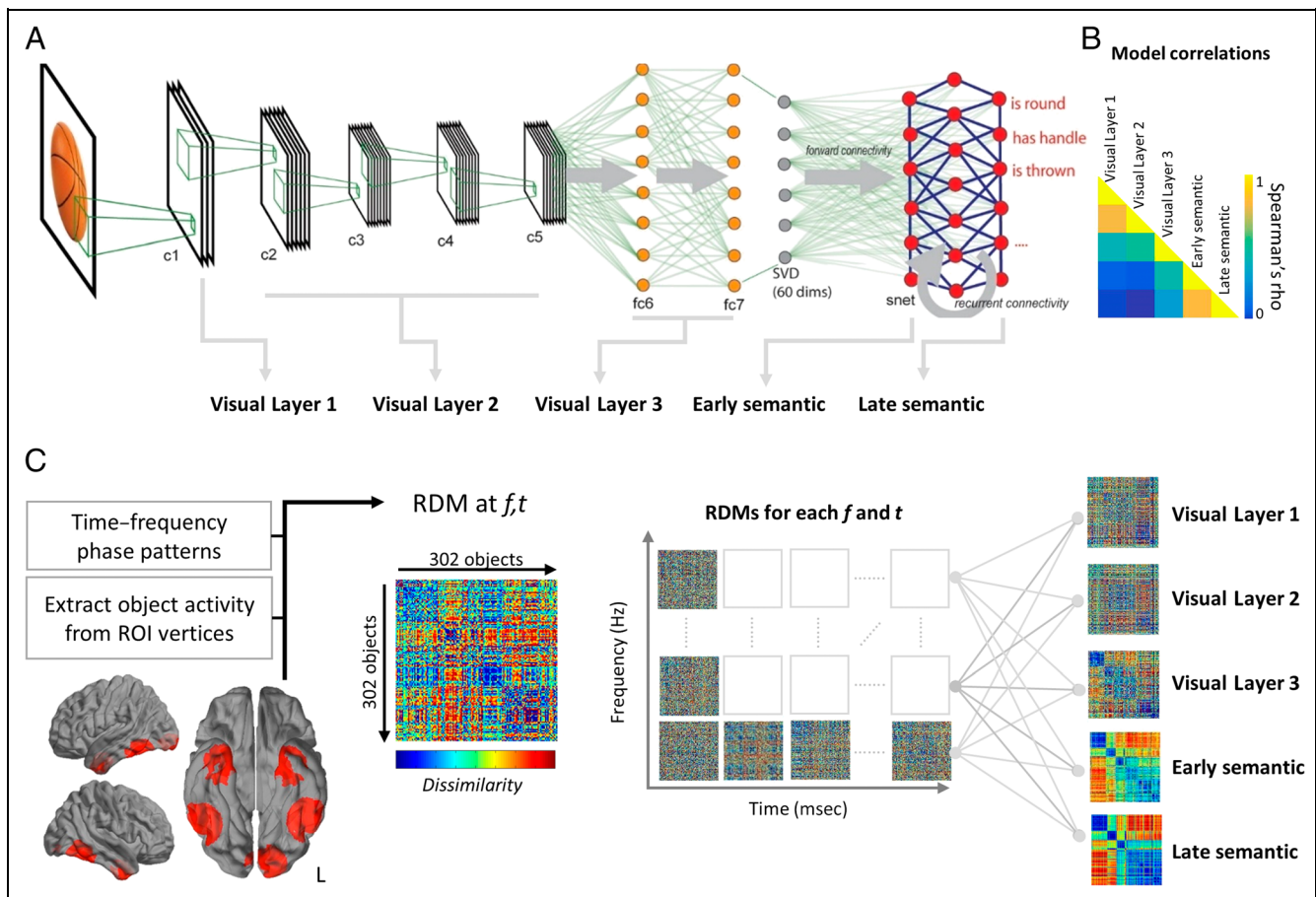


Figure 1. RSA using computational models and oscillations. (A) The combined visual DNN and semantic AN models the low-level visual properties of the input and higher-level image properties that increase in complexity across Layers c1 to fc7. The visual properties in fc7 then map onto a recurrent AN that activates the semantic features associated with the input. In our analyses, we combined layers of the DNN into three visual model RDMs and combined the AN into two semantic model RDMs capturing increasingly specific visual and semantic information. (B) Correlations between the different visual and semantic model RDMs. (C) RSA analysis of time–frequency data. Spatiotemporal activity patterns are extracted from an ROI for each object. Time–frequency phase is calculated for each ROI, and RDMs are created for each point in time and for each frequency. Each RDM is then correlated with each RDM from the computational model to test when and at what frequency different object properties are represented in oscillatory phase patterns. The procedure is then repeated for all ROIs.

semantic information may be more associated with theta activity (Halgren et al., 2015) and gamma activity (Mollo, Cornelissen, Millman, Ellis, & Jefferies, 2017; Supp, Schlogl, Trujillo-Barreto, Müller, & Gruber, 2007).

METHODS

We reanalyzed MEG data reported in Clarke et al. (2015) and thus only summarize the main aspects of study design here.

Participants and Procedure

Fourteen individuals took part in the study. Two participants were excluded from the analysis because of poor source reconstruction results (failure to show occipital activity ~100 msec after onset of object), leaving 12 participants in the analysis. Participants performed a basic-level naming task (e.g., “tiger”), with 302 common objects from a diverse range of superordinate categories

including animals, clothing, food, musical instruments, tools, and vehicles. All objects were presented in color as single objects on a white background. Each trial began with a black fixation cross on a white background for 500 msec before the object was shown for 500 msec, followed by a blank screen lasting between 2400 and 2700 msec. The order of stimuli was pseudorandomized.

MEG/MRI Recording

Continuous MEG data were recorded using a whole-head 306 channel (102 magnetometers, 204 planar gradiometers) Vectorview system (Elekta Neuromag) located at the MRC Cognition and Brain Sciences Unit, Cambridge, UK. Eye movements and blinks were monitored with EOG electrodes placed around the eyes, and five head position indicator coils were used to record the head position (every 200 msec) within the MEG helmet. The participants’ head shape was digitally recorded using a 3-D digitizer (Fastrak Polhemus, Inc.), along with the positions

of the EOG electrodes, head position indicator coils, and fiducial points. MEG signals were recorded at a sampling rate of 1000 Hz, with a band-pass filter from 0.03 to 125 Hz. To facilitate source reconstruction, 1 mm³ T1-weighted MPRAGE scans were acquired during a separate session with a Siemens 3T Tim Trio scanner (Siemens Medical Solutions) located at the MRC Cognition and Brain Sciences Unit, Cambridge, UK.

MEG Preprocessing

Initial processing of the raw data used MaxFilter Version 2.0 (Elektra-Neuromag) to detect bad channels that were subsequently reconstructed by interpolating neighboring channels. The temporal extension of the signal-space separation technique was applied to the data every 10 sec to segregate the signals originating from within the participants' head from those generated by external sources of noise. A correlation limit of .6 was used as this has been shown to additionally remove noise from close to the head, as produced during speech (Medvedovsky, Taulu, Bickmullina, Ahonen, & Paetau, 2009), and head movement compensation was applied. The resulting MEG data were low-pass filtered at 200 Hz in forward and reverse directions using a fifth-order Butterworth digital filter and high-pass filtered at 0.1 Hz using a fourth-order Butterworth filter, and residual line noise was removed with a fifth-order Butterworth stop-band filter between 48 and 52 Hz. Data were epoched from -1.5 to 2 sec and downsampled to 500 Hz using SPM12 (Wellcome Institute of Imaging Neuroscience).

Independent components analysis (ICA) was used to remove artifactual signals, using *runica* implemented in EEGLab (Delorme & Makeig, 2004) and SASICA (Chaumon, Bishop, & Busch, 2015). ICA was performed separately for magnetometers and gradiometers with 60 components for each. Components of the data that showed a Pearson's correlation greater .4 with either EOG channel were removed from the data, as were components correlated with the ECG recording. SASICA and FASTER were additionally used to identify components related to muscle and high-frequency artifacts, and components that showed a rising profile of evoked activity between 200 msec and 1 sec were removed (these characterize speech artifacts; mean naming latency 991 msec, *SD* = 109 msec). All components were visually inspected to confirm removal, as recommended (Chaumon et al., 2015). After ICA, a baseline correction was applied to all trials using data from -500 to 0 msec. Items that were incorrectly named were excluded, where an incorrect name was defined as a response that did not match the correct concept.

Source Localization

Source localization of MEG signals used a minimum-norm procedure applied in SPM12. First, the participants' MRI images were segmented and spatially normalized to

a Montreal Neurological Institute (MNI) template brain. A template cortical mesh with 8196 vertices was inverse-normalized to the individual's specific MRI space. MEG sensor locations were coregistered to MRI space using the fiducial points and digitized head points obtained during acquisition. The forward model was created using the single shell option to calculate the lead fields for the sources oriented normal to the cortical surface (including a lead field correction following ICA; Hipp & Siegel, 2015). The data from both magnetometers and gradiometers were inverted together using the group inversion approach to estimate activity at each cortical vertex using a minimum norm solution (MIM). A frequency window of 0–150 Hz was specified, and no hanning window was applied.

Representational Similarity Analysis

RSA was used to compare the similarity/distances between objects based on computational models and the similarity derived from oscillatory patterns. This requires that we calculate representational dissimilarity matrices (RDMs) from both the computational model layers and from source-localized MEG signals.

RDMs from Computational Models

The computational models used here are those that have been successfully used to describe the gradient of visual to semantic object representations along the VVP in fMRI (Devereux et al., 2018).

Visual DNN. We used the DNN model of Krizhevsky et al. (2012), as implemented in the Caffe deep learning framework (Jia et al., 2014), and trained on the ILSVRC12 classification data set from ImageNet. We used the first seven layers of the DNN, consisting of five convolutional layers (conv1–conv5) followed by two fully connected layers (fc6 and fc7). The convolutional kernels learned in each convolutional layer correspond to filters receptive to particular kinds of visual input. In the first convolutional layer, the filters reflect low-level properties of stimuli and include one sensitive to edges of particular spatial frequency and orientation, as well as filters selective for particular color patches and color gradients (Zeiler & Fergus, 2014; Krizhevsky et al., 2012). Later DNN layers are sensitive to more complex visual information, such as the presence of specific visual objects or object parts (e.g., faces of dogs, legs of dogs, eyes of birds, and reptiles; see Zeiler & Fergus, 2014), irrespective of spatial scale, angle of view, and so forth. We presented 627 images to the pretrained network (including the 302 images presented to participants), where each image represented a concept listed in a large property norm corpus (Devereux, Tyler, Geertzen, & Randall, 2014). This produced activation values for all nodes in each layer of the network for each image.

To create RDMs for each layer of the DNN, we first applied PCA to reduce the dimensionality of each layer while keeping the components that explained 100% of the variance. For example, fc6 has 4096 nodes, and after PCA each of the 627 object images was represented by a 626 length vector. This was found to dramatically improve the relationship between MEG signals and the DNN, which may be because the white space surrounding images was reduced from being represented across a large number of nodes to a few components, meaning the similarity between objects was focused on the areas of the images where the objects appeared. Although the PCA improved the relationship between MEG signals and the DNN for objects isolated from backgrounds, this would not be expected for naturalistic images. Following PCA, we excluded all object activations that were not in this study, leaving 302.

As many of the layers were highly correlated and to reduce the number of RDMs tested, subsets of the seven layers were combined. The object activation matrices were concatenated across layers, and the dissimilarity between network activity for different object images was calculated as $1 - \text{Pearson's correlation}$. This was applied to conv1, concatenated activations from conv2 to conv5, and concatenated activations from fc6 to fc7, which are referred to as visual Layers 1, 2, and 3, respectively. A model RDM was also created based on concatenated data from all layers of the DNN.

Semantic AN. DNNs have proven effective in labeling object images in complex contexts. However visual DNNs do not capture object semantics because, although they can find the correct labels for images, they do not capture how different objects are semantically related to one another (e.g., that a dog and a cat are related in meaning) and only takes into account the similarity of their visual properties, rather than also taking into account nonvisual and functional information (Devereux et al., 2018). To provide one potential route for the relationship between higher-level visual properties and semantic properties, we use the output from the DNN as input to an AN model of semantics.

Our semantic knowledge of concrete concepts can be captured by distributed semantic feature models (Taylor, Devereux, & Tyler, 2011; Rogers & McClelland, 2004; Cree & McRae, 2003; Tyler & Moss, 2001), where each concept is represented by a set of features—for example, *is shiny, has a handle, used for chopping* are features of a knife from the property norming corpus of Devereux et al. (2014). Based on semantic features, the similarity between concepts is accounted for on the basis of the features they share, whereas distinctive features allow for differentiation between items (Taylor et al., 2011). The semantics of the 627 object concepts from the property norms can be represented across 2469 semantic features, and in the AN, these correspond to the 2469 nodes. The AN was based on Cree et al. (2006) and

was trained to activate the correct pattern of semantic features from the inputs from the DNN (full details in Devereux et al., 2018). The network was trained using continuous recurrent back-propagation through time over 20 processing time-ticks. As input to the AN, we took the activation over the 4096 nodes of fc7 and reduced this to 60 dimensions using singular-value decomposition (SVD) (note that RDMs calculated on the full-dimensional fc7 and the SVD-reduced layer were highly correlated, Spearman's $\rho = 0.98$, indicating no substantial information loss). After training, over the 20 time-ticks, the semantic features associated with the concept are gradually activated, with the speed of activation depending on the relationship to the visual features and the statistical regularities between features (i.e., whether a certain combination of features predicts the occurrence of another feature). Thus, early features to activate are shared features and visual features, followed by nonvisual and distinctive features. For further implementation details, see Cree et al. (2006) and Devereux et al. (2018).

Like with the visual DNN, many of the 19 layers of the AN (discounting the input layer) are highly correlated and so were combined. Using *k*-means clustering, the 19 layers could be described well by two principal groups, as shown by positive silhouette values. Clustering solutions with one, three, four, or five groups all contained negative silhouette values showing that two provided the most optimal number of clusters. After PCA, Layers 1–5 were concatenated, and Layers 6–19 were concatenated. The dissimilarity between AN activity for different object images was calculated as $1 - \text{Pearson's correlation}$, giving an early semantic RDM and a late semantic RDM. An additional semantic RDM was created based on the concatenation of all 19 layers.

RDMs from Time–Frequency Signals

Object dissimilarity from MEG signals was based on oscillatory phase patterns from source-localized data. Five ROIs were specified covering locations known to be sensitive to visual and semantic object properties; each ROI was specified by a coordinate and radius of 20 mm: occipital pole (MNI: $-10, -94, -16$), left pVTC (MNI: $-50, -52, -20$), right pVTC (MNI: $52, -56, -16$), left ATL (MNI: $-30, -6, -40$), and right ATL (MNI: $30, -4, -42$). Coordinates were defined based on local maxima of source-localized activity to all objects. Within each ROI (defined by the center coordinate and radius), single trial activity was extracted for each vertex. Instantaneous phase was calculated for each trial and for every vertex using Morlet wavelets using the *timefreq* function in EEGLAB. Phase was extracted between -700 and 1000 msec in 20-msec time steps and between 4 and 95 Hz in 50 logarithmically spaced frequency steps. A five-cycle wavelet was used at the lowest frequency, increasing to a 15-cycle wavelet at the highest. This produced a time–frequency representation (TFR) for every trial at every vertex location

in the ROI. RDMs between object TFRs were calculated at each time–frequency point using the circular distance (Berens, 2009) between vectors of phase information over space (vertices) and over 60 msec.

For analyses at distinct frequency bands rather than at every frequency, the oscillatory RDMs were averaged across frequencies. The frequencies within each band were defined using hierarchical clustering in sensor space, with the aim of allowing the data to define the boundaries between different bands (also see Crivelli-Decker, Hsieh, Clarke, & Ranganath, 2018). TFRs were computed for each MEG sensor, which were averaged across all trials and participants to produce a grand average for each sensor. A vector was created for each frequency that included all time points and sensors concatenated before hierarchical clustering of frequencies using correlation as the distance measure. The resulting distances were visualized as a dendrogram to define the boundaries of the different bands. This resulted in theta (4–9 Hz), alpha (9–15 Hz), beta (16–30 Hz), and gamma (30–95 Hz).

RSA Statistics

Each RDM based on oscillatory phase signals was correlated with the RDMs from the computational models using Spearman's correlation (Spearman's correlation was used to be consistent with prior publications using similar data and model RDMs; Devereux et al., 2018; Clarke & Tyler, 2014). This resulted in TFRs that captured the relationship between phase information and the visual and semantic network models. RSA TFRs were calculated for each layer, ROI, and participant. Random effects analysis testing for positive RSA effects was conducted for each time–frequency point using one-sample t tests against zero ($\alpha = .01$). Only positive RSA effects were tested as we are interested in when the similarity structure in neural signals relate to the similarity structure predicted by visual and semantic RDMs.

Cluster mass permutation testing was used to assign p values to clusters of significant tests (Maris & Oostenveld, 2007), and a maximum cluster approach was used to control for multiple comparisons across time, frequency, ROI, and model RDM (Nichols & Holmes, 2002). For each permutation, the sign of the TFR correlations was randomly flipped for each participant before one-sample t tests of the permuted data at each time and frequency point. To construct the null distribution for the maximum cluster approach, the same permutation scheme was applied to all ROIs and model RDMs, and the largest cluster (sum of above-threshold t values) from any ROI and models was retained for the null distribution and repeated 10,000 times. The cluster p value for each of the observed cluster in the original data was defined as the proportion of the 10,000 permutation cluster masses (plus the observed cluster mass) that is greater than or equal to the observed cluster mass. Using this approach,

we correct for the total number of statistical comparisons performed over all time points, frequencies, each ROI, and all model RDMs tested.

Peak RSA Effects

To determine when different kinds of information were present relative to one another, we determined when the peak effects occurred across different regions for different visual and semantic RDMs. This analysis was performed for RSA effects within each frequency band, in addition to peak effects collapsing across frequencies. The latency of the peak was defined as the maximum Spearman's correlation value between 50 and 500 msec. A latency was found for each frequency band, model RDM, and ROI. Linear mixed effects (LME) models were used to test the relationship between the peak latency, and ROI and computational model layer. The peak frequency analysis was based on RSA effects determined across the full frequency spectrum. The peak was defined as the frequency of the maximal RSA effect between 50 and 500 msec. In both latency and frequency analyses, LME models (using `fitlme`) were used to test the relationship between the peaks, and ROI and computational model layer. For visualization, peaks are plotted as probability density functions and using `gramm` (<https://doi.org/10.5281/zenodo.59786>). Finally, we did not control for the number of LME models performed ($n = 3$ for temporal peaks, $n = 4$ for frequency peaks).

Granger Causality

Finally, we tested the causal relationships between RSA effects seen for visual and semantic properties and across different ROIs. Specifically, we used Granger causality (GC) analysis to test if RSA time courses in one region have a subsequent impact on RSA time courses in other regions. To aid interpretability, GC analysis was applied to the RSA time courses averaged across frequency bands and for the concatenated visual and concatenated semantic model RDMs. GC was calculated between the five ROIs and the two RSA time courses (10 time series in total). Each time series was the RSA effect between 50 and 500 msec concatenated across participants. Time domain GC used the multivariate GC toolbox (Barnett & Seth, 2014), with a model order of 2 (40 msec) as indicated by the Akaike information criterion (AIC) for model order estimation. To remove bias in the resulting GC values, surrogate data were used to estimate the bias and remove it from the GC values. The data were divided into time windows (of length model order) and randomly rearranged creating 5000 surrogate data sets. The mean GC across the surrogate data was used as an estimate of the bias and subtracted from the original GC values. This approach is considered to debias the GC values (Barnett & Seth, 2014; Barrett et al., 2012). Granger F tests were applied to the unbiased pairwise conditional GC values, and multiple

comparisons correction used false discovery rate (FDR) and an alpha of .05 for a total of 90 pairwise connections.

RESULTS

Our primary goal was to test how the VVP represents increasingly complex visual and semantic information over time. To achieve this, we used RSA to test if the visual and semantic information, extracted from the computational models, was represented in spatiotemporal patterns of oscillatory phase from source-localized MEG signals. We analyzed data from five ROIs covering occipital, pVTC, and the ATL, which are known to be primarily implicated in the processing of visual and semantic object properties.

Time–frequency RSA (TF RSA) showed that neural patterns based on oscillatory phase had a significant relationship to both the visual and semantic models. The effects were concentrated in the first 500 msec and seen across theta, alpha, and beta frequencies (Table 1). We first present a brief overview of visual and semantic effects

before a more detailed follow-up analysis of the timing and frequencies of the effects.

Visual Models

TF RSA effects were seen for all three visual models in each ROI across theta, alpha, and beta frequencies and strongest in the occipital ROI (Figure 2). It is predicted that early or intermediate visual layers will be the best predictors of occipital responses, and more anterior regions will be best captured by the last visual layer. Planned contrasts showed the effects were significantly greater for visual-layer 2 compared with visual-layer 1 ($t = 4.56, p < .001$) with no difference between visual Layers 2 and 3 ($t = 0.27$). In higher regions along the ventral stream, visual Layer 3 had a significantly greater fit than both Layer 2 (left pVTC [LpVTC]: $t = 4.05, p = .002$; right pVTC [RpVTC]: $t = 4.30, p = .001$; left ATL [LATL]: $t = 3.35, p = .006$; right ATL [RATL]: $t = 3.64, p = .004$) and Layer 1 (LpVTC: $t = 4.90, p < .001$; RpVTC: $t = 7.00, p < .0001$; RATL: $t = 7.35, p < .0001$), except in

Table 1. TF RSA Results

<i>Models</i>	<i>ROI</i>	<i>Freqs</i>	<i>Times</i>	<i>Mass</i>	<i>Cluster p</i>
Visual Layer 1	Occip	4–50 Hz	0–730 msec	4857	.0002
Visual Layer 1	LpVTC	4–15 Hz	0–610 msec	1392	.0073
Visual Layer 1	RpVTC	4–15 Hz	0–350 msec	1364	.0077
Visual Layer 1	LATL	4–14 Hz	0–410 msec	1379	.0077
Visual Layer 1	RATL	7–15 Hz	10–370 msec	369	.0365
Visual Layer 1	RATL	4–6 Hz	70–350 msec	233	.1001
Visual Layer 2	Occip	4–34 Hz	0–750 msec	5343	.0002
Visual Layer 2	LpVTC	4–16 Hz	0–630 msec	1522	.0051
Visual Layer 2	RpVTC	4–21 Hz	0–770 msec	2093	.0035
Visual Layer 2	LATL	4–14 Hz	0–390 msec	1378	.0077
Visual Layer 2	RATL	4–15 Hz	0–750 msec	1298	.0079
Visual Layer 3	Occip	4–32 Hz	0–910 msec	5599	.0001
Visual Layer 3	LpVTC	4–23 Hz	0–690 msec	2301	.0030
Visual Layer 3	RpVTC	4–23 Hz	0–730 msec	3033	.0018
Visual Layer 3	LATL	4–18 Hz	0–590 msec	1955	.0036
Visual layer 3	RATL	4–17 Hz	0–690 msec	1943	.0036
Early semantic	Occip	5–14 Hz	0–690 msec	701	.0145
Early semantic	LpVTC	4–6 Hz	170–450 msec	251	.0843
Early semantic	RpVTC	12–21 Hz	110–390 msec	231	.1014
Early semantic	LATL	4–8 Hz	0–450 msec	584	.0181
Late semantic	LpVTC	4–8 Hz	0–630 msec	585	.0181
Late semantic	LATL	4–7 Hz	0–390 msec	447	.0262

Boldface indicates $p < .05$.

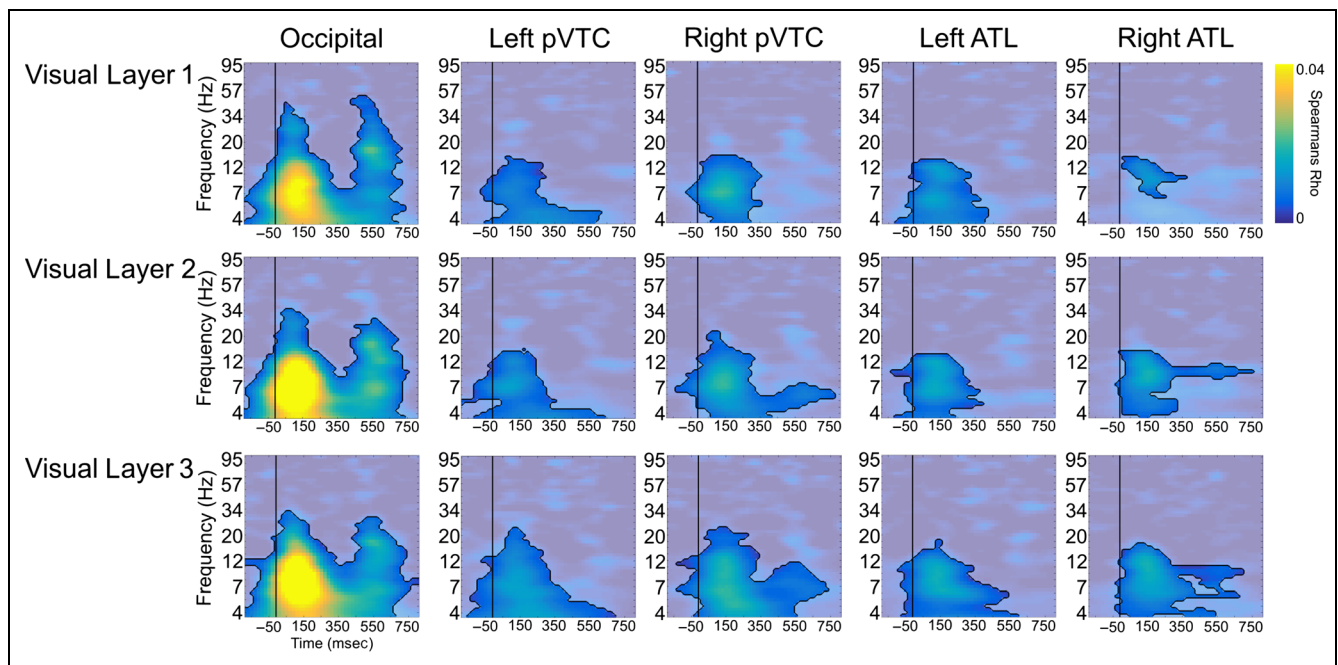


Figure 2. TF RSA effects of the visual DNN. Each plot shows the Spearman's correlation values between an RDM from the visual DNN and each ROI. Significant clusters are shown outlined in black, using a threshold of $p < .01$ at the pixel level and $p < .05$ at the cluster level (corrected for all ROIs and model RDMs tested). Nonsignificant time–frequency points are displayed in the background. Black line shows 0 msec.

the LATL ($t = 2.01$, $p = .07$). These results are in line with predictions that later regions along the ventral stream represent more complex visual object information that is, in turn, better captured by later layers of the visual DNN.

Semantic Models

TF RSA analysis of phase showed significant effects for both semantic models (Figure 3). Both the early-semantic and late-semantic models were significantly related to spatiotemporal phase patterns in the LATL in theta frequencies during the first 400 msec. Furthermore, the

early-semantic model had a significantly better fit compared with the late-semantic model in LATL ($t = 2.96$, $p = .013$). The early-semantic model was also significantly related to occipital phase patterns in theta and alpha frequencies. Finally, the late-semantic model was significantly related to the LpVTC in theta frequencies. These results show that semantic information about objects is captured through oscillatory phase patterns in the ventral stream, with the most prominent effects in theta in the pVTC and the ATL—key regions supporting object semantic information over time (Clarke et al., 2011, 2015; Clarke & Tyler, 2014).

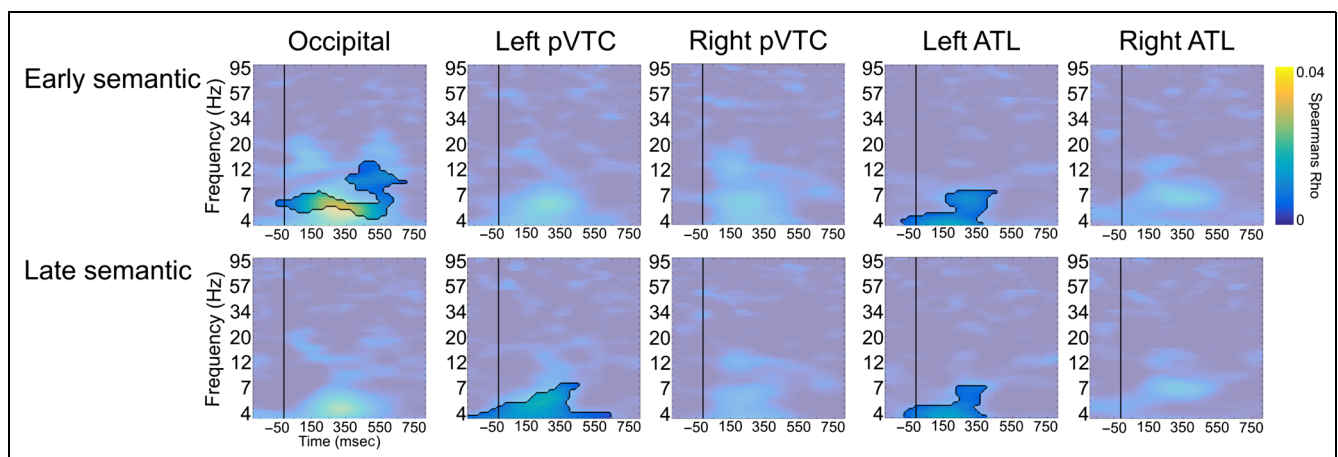


Figure 3. TF RSA effects of the semantic AN. Plots show the Spearman's correlation values between a semantic AN RDM and each ROI. Significant clusters are shown outlined in black, using a threshold of $p < .01$ at the pixel level and $p < .05$ at the cluster level (corrected for all ROIs and model RDMs tested). Nonsignificant time–frequency points are displayed in the background. Black line shows 0 msec.

Representational Changes over Time

Our analysis so far shows that the combined visual DNN and semantic AN models are capturing neural processes along the VVP. We next sought to determine the relative changes in object information over time and region. However, it is difficult to establish when different forms of information are present based on the onsets of significant effects because of the temporal smearing wavelet convolution creates—especially at lower frequencies—and the use of a spatiotemporal sliding window that further contributes to a smoother pattern. Furthermore, onsets cannot be easily compared across different frequencies as the temporal smearing is greater at lower compared with higher frequencies. Therefore, to determine when different kinds of information are present relative to one another, we analyzed when the peak effects occurred across different regions for different visual and semantic models. We used LME models to test the relationship between the peak time of RSA effects and the layer of the computational model (modeled from visual Layer 1, Layer 2, Layer 3, early semantics, late semantics) and hierarchical cortical level of the VVP (occipital, pVTC, ATL; where left and right hemispheres are combined).

We found a significant effect of cortical level, in that later levels of the VVP had later peak RSA effects (Beta coefficient: 26 msec, $SE = 6.7$ msec, $t = 3.90$, $p = .0001$; Figure 4A) and a significant effect of computational model layer in that later layers had significantly later peaks (Beta coefficient: 30 msec, $SE = 3.6$ msec, $t = 8.34$, $p < .0001$; Figure 4B). Furthermore, as shown in Figure 4B, there was a prominent separation in the timing of visual and semantic peak effects. A subsequent LME model combined the data within visual and semantic models and showed that semantic effects lagged visual effects by an estimated 88 msec ($t = 8.12$, $p < .0001$).

After establishing this broad pattern where effects are later in time for higher regions of the VVP and for later layers of the visual-to-semantic model, we next tested for region-specific changes in the latency of peak RSA effects within three frequency bands that showed significant effects—theta, alpha, and beta. Separate LME models were run for each cortical level of the VVP for each frequency band. Significant positive effects of model layer were seen in the occipital and pVTC for theta, alpha, and beta, whereas the ATL showed significant positive effects in theta and alpha (Figure 4C–E). This establishes that later layers of the combined computational model showed later peak RSA effects in theta, alpha,

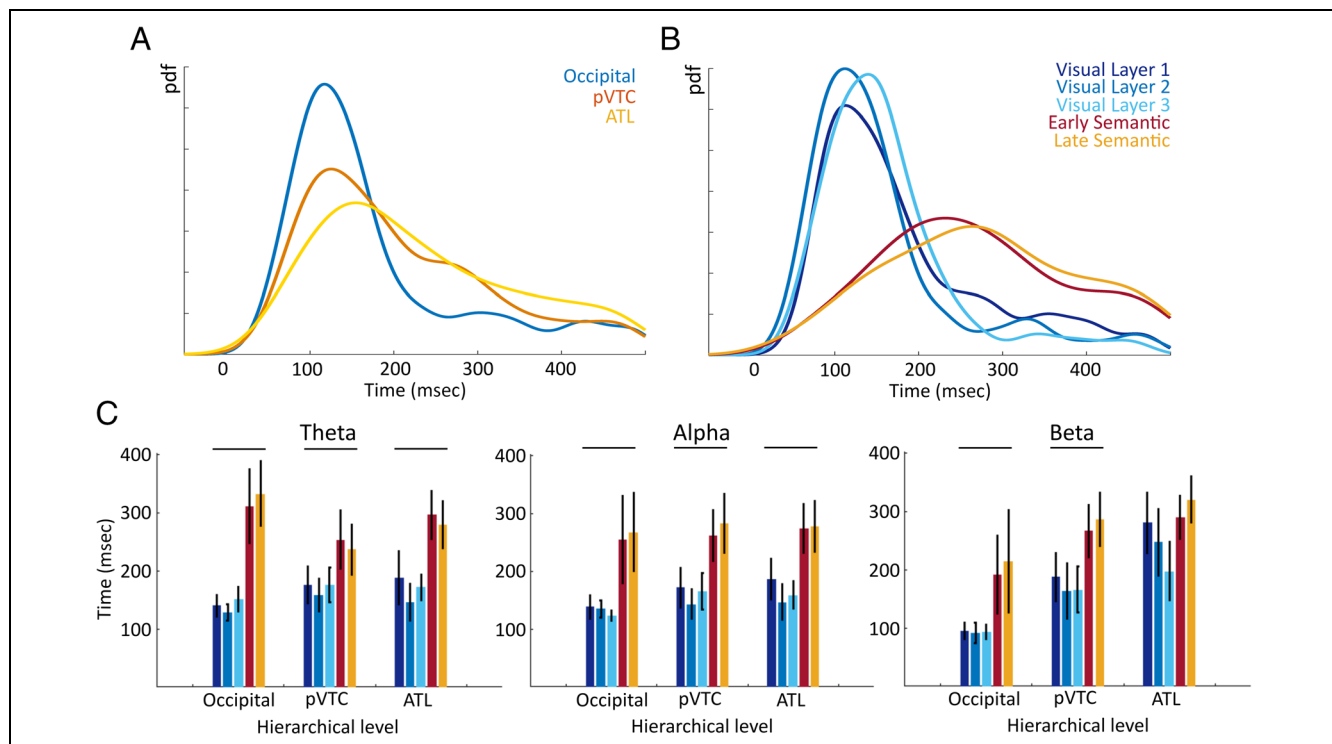


Figure 4. Temporal peaks for the visual DNN and semantic AN RSA effects. (A) Probability density plot showing that the latencies of the peak RSA effects follow the hierarchical levels of the VVP (data combined across hemispheres and model RDMs). (B) Probability density plot showing that the latencies of the peak RSA effects for different model RDMs have a clear distinction between visual DNN and semantic AN latencies whereas later model layers tend to have later peaks. (C–E) Mean peak latencies for different model RDMs at each hierarchical level for three frequency bands where significant RSA effects were present. Plots show a general increase in latency across the models from visual to semantic (colors match those in B). Horizontal lines indicate a significant linear relationship between latency and model layer.

and beta frequencies across all levels of the VVP, supporting our broad results of a temporal transition from visual to semantics over time in accordance with the changes seen over the successive layers of the computational model.

Representational Changes over Frequency

We next tested how the peak frequency of the RSA effects changed. Using an LME model, we found a marginal effect of hierarchical cortical level (Beta coefficient = 2.2 Hz, $SE = 1.1$, $t = 1.89$, $p = .06$), but not of model layer ($p = .21$). The interaction between level and model was trending toward significance ($t = 1.95$, $p = .053$). To explore the interaction, separate LME models were run for each hierarchical level testing for an effect of model layer. Only the ATL showed a significant effect of model layer, where later layers of the visual-to-semantic model had lower peak frequencies (Beta coefficient: -0.74 Hz, $t = 2.02$, $p = .046$; Figure 5). As shown in Figure 5, plotting the probability density across frequencies suggests semantic models have median peak frequency around 5–6 Hz whereas visual models have peaks closer to 10 Hz, suggesting an alpha–theta distinction between vision and semantics.

Direction of Information Flow

The results presented so far show a visual to semantic trajectory through time and space, where effects are later in time for higher regions of the VVP and for later layers of the visual-to-semantic model. However, focusing solely on peak effects will not fully capture the ongoing dynamics and critically does not tell us about the connectivity relationships between regions or information types. To address this, we used GC analysis to test if representations

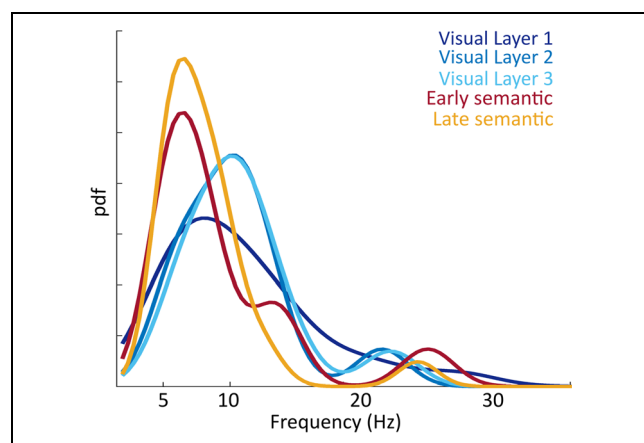


Figure 5. Spectral peaks for the visual DNN and semantic AN RSA effects in the ATL. Probability density plot showing that the peak frequency of RSA effects shows a clear distinction between visual and semantic model RDMS, where visual effects peak near 10 Hz and semantic effects peak near 5 Hz.

in one region have a subsequent impact on representations in other regions. For example, GC with RSA time courses allows us to test if visual information in one region has a Granger causal impact on subsequent visual representations in a different region or whether visual representations have a Granger causal impact on subsequent semantic representations. GC analysis was applied to the RSA time courses averaged across theta and alpha bands (this was because the effects were concentrated in these low frequencies and therefore reflects the dominant visual and semantic effects) to test for GC relationships between visual representations across regions, semantic representations across regions, and critically between visual and semantic representations both within and across regions. For this analysis, we focus on RSA effects from the combined visual and combined semantic RDMS (Figure 6).

We first tested how visual RSA effects impact visual effects in other regions (Figure 6C). Significant feedforward GC was seen between the occipital region and all other regions. This suggests that visual representations in the occipital lobe have an impact on subsequent visual representations further along the VVP in accordance with feedforward models of visual processing. Semantic RSA effects (Figure 6D) showed significant feedforward, cross-hemispheric, and feedback connectivity, with both the left and right ATL playing prominent roles. Semantic effects in the LATL significantly influenced later semantic effects in more posterior regions, whereas the RATL showed significant connectivity from bilateral pVTC. In addition, bidirectional connectivity was seen between the ATL regions. This shows that, in contrast to visual RSA connectivity, the spread of semantic effects were associated with more complex feedforward, feedback, and cross-hemispheric connectivity.

Crucially, we tested the relationships between visual and semantic RSA effects (Figure 6E) by testing if visual RSA effects in one region influenced later semantic effects in other regions (or the same region) and vice versa. Visual RSA effects emanating from the occipital and RpVTC significantly influenced semantic effects through feedforward connectivity with the ATL, whereas visual RSA effects from the occipital region also influenced later semantic effects in the RpVTC. The occipital visual RSA effects influenced later semantics in the occipital, whereas visual effects in the LpVTC also influenced later semantic effects in the LpVTC. Finally, visual RSA effects in the ATL influenced later semantic effects in the pVTC through feedback connectivity, an effect that was present in both hemispheres. This shows a pattern where feedforward visual-to-semantic transformations occur from the occipital to LATL and along the right VVP. Feedback visual-to-semantic transformations occurred from the ATL to pVTC bilaterally, in addition to a shifting visual-to-semantic representation within LpVTC. Lastly, semantic RSA effects had a significant effect on visual representations (Figure 6F) in the RpVTC and from RpVTC to LpVTC. Overall, the GC results show that feedforward processing in the VVP supports the dynamic

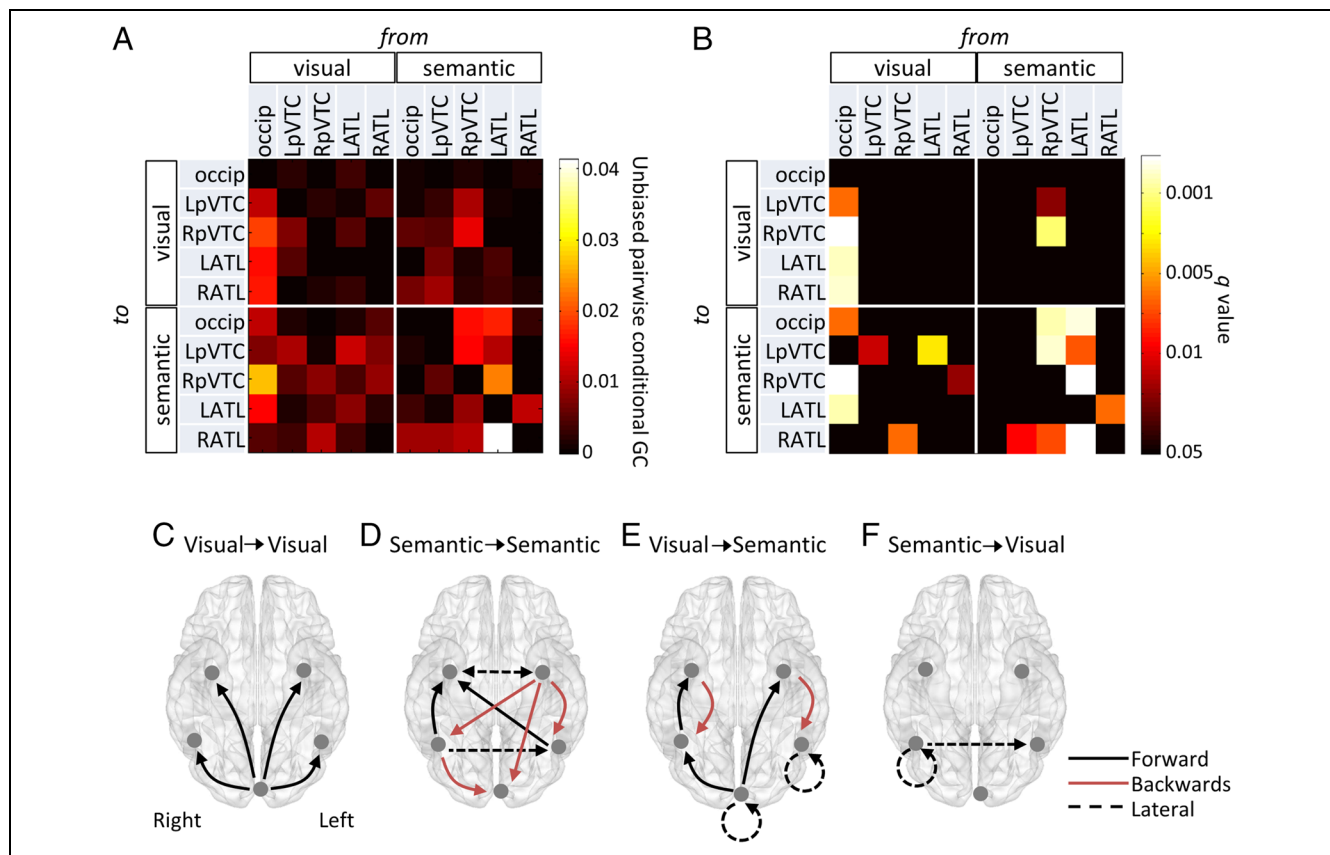


Figure 6. GC of RSA time courses. (A) All pairwise GC values after removing the common dependencies from other regions. (B) Significance of GC values, showing q values (FDR-corrected p values) less than 0.05. (C–F) Images show significant GC of the RSA time courses between regions. Each image shows how RSA effects in one region impact future RSA effects in another region. The analysis was conducted both for RSA effects across regions within the visual DNN or semantic AN model RDMS (left two images) and when the RSA effects of the visual DNN could show GC with RSA effects with the semantic AN (and vice versa; right two images). Significant connections shown using $p < .05$, FDR-corrected.

processing of visual information whereas combination of feedforward and feedback is more central for semantics. We also highlight that visual to semantic information transitions engage feedforward and feedback connectivity, with the ATL appearing as a vital region.

DISCUSSION

In this study, we successfully combined RSA for time-frequency phase information with a computational architecture for visual to semantic processing. Utilizing a combined visual DNN and semantic AN, we were able to demonstrate how the incremental aspects of visual to semantic processes occur in the ventral stream over time and the underlying dynamics supporting this transition. We report several novel additions. First, that TF RSA revealed visual and semantic object properties were reflected in low-frequency phase activity in the VVP. As would be expected, spatial and temporal hierarchies were apparent, where later layers of the computational model showed peak effects later in time and in later regions along the posterior to anterior axis. Second, we also revealed that more subtle dynamics underlie recognition, where feedforward connectivity supported the

transfer of visual information in the VVP and combined feedforward, feedback, and intraregion dynamics supported the transition between visual and semantic information processing states. This was revealed through a novel application of GC to RSA time courses. And third, our analysis suggests a novel hypothesis that the ATL codes visual and semantic properties through a multiplexed code. These results present the first detailed account of how oscillatory dynamics can support the emergence of meaning from visual inputs.

Here we used TF RSA with oscillatory phase information, showing that low-frequency phase carries stimulus-specific information related to visual and semantic object properties. The analysis was based on phase patterns from MEG source-localized data, with our results showing that objects with more similar properties have more similar spatiotemporal phase patterns in the mass signals recorded through MEG. It is believed that the phase of low-frequency activity is suited for decoding stimulus properties for MEG, EEG, and electrocorticography (ECOG) (Panzeri, Macke, Gross, & Kayser, 2015; Watrous, Fell, et al., 2015), supported by a number of studies showing that oscillatory phase carries more information about the stimulus than power (Staudigl et al., 2015; Lopour et al., 2013; Ng

et al., 2013; Schyns et al., 2011). Although not presented here, we also see a similar pattern with our data. Although neural mass activity can be difficult to relate to the underlying neural activity, there is some suggestion that low-frequency phase of mass signals might index the timing of the underlying neural activity and its firing (Panzeri et al., 2015; Watrous, Fell, et al., 2015; Montemurro et al., 2008). As such, our effects based on spatiotemporal phase patterns may be driven by spatiotemporal activity patterns of the mass neural populations and further suggest that cognitively relevant properties are coded in distributed neural activity patterns in space and time. However, the relative importance of a spatial or temporal activity patterns for object properties was not determined in this study.

Previous studies in both humans and nonhuman primates have identified category-specific phase coding of objects, where different object categories have different preferred phases associated with neural activity (Watrous, Deuker, et al., 2015; Turesson et al., 2012). Here, we go beyond phase dissociations between different categories by showing that the variability in phase information relates to variability in the stimulus properties and is the case for both visual and semantic properties. We see that low-frequency phase patterns, peaking in alpha, most strongly relate to visual properties from the DNN, and phase patterns peaking in theta relate to semantics. Low-frequency activity over posterior regions is linked to perceptual cycles that structure visual processing of objects (Jensen et al., 2014; VanRullen et al., 2014; Kayser et al., 2012), and such low-frequency phase patterns have been shown to relate to content-specific visual information in the occipital lobe (Michelmann et al., 2016). Alpha activity is claimed to reflect a pulsed inhibition of cortical activity, where increases in alpha power result in the inhibition of a region and decreased alpha power relates to the active engagement of a region (Jensen & Mazaheri, 2010; Klimesch, Sauseng, & Hanslmayr, 2007). Research using combined EEG and fMRI has further shown that occipital alpha power reductions correlated with increased BOLD in downstream object processing regions (Zumer, Scheeringa, Schoffelen, Norris, & Jensen, 2014), and so alpha activity could organize the flow of information through the VVP, as supported through our connectivity analysis (see below). However, it is also worth noting that effects of the DNN, although peaking in alpha, were seen across theta, alpha, and beta frequencies, which may instead highlight the important role of low-frequency oscillations for perceptual processing rather than only relating to alpha activity.

Some of the RSA effects we observed temporally overlap with typically reported event-related components seen in EEG and MEG. This might suggest that our analysis is picking up on the phase-locked aspects of the signal (that will contribute to the event-related component); however, given that our analysis depends on a statistical correspondence between phase variability and the

variability produced by the computational models, our results cannot be driven solely by the phase-locked aspects of the signal. To illustrate, a phase-locked evoked response in all trials (whether produced through phase resetting or an additive model) would result in little variability in phase over trials, and as our RSA analysis depends on variability in phase angle over trials, our analysis must also be picking up non-phase-locked aspects of the signal. Overall, our phase-based RSA analysis is likely driven by variability in the timing of the underlying neural activity that we see through variability in phase patterns generated by the stimulus (Panzeri et al., 2015; Watrous, Fell, et al., 2015; Montemurro et al., 2008).

Both alpha and theta activities are sometimes considered to have similar roles in organizing neural activity (Jensen et al., 2014; Lisman & Jensen, 2013). Both alpha and theta activities are modulated by memory, but often with opposing effects (Hanslmayr et al., 2012), and our clustering of frequencies to generate the different bands revealed separate clusters for theta and alpha. Together, this suggests a functional dissociation between theta and alpha in cortex. Theta activity in the hippocampus and medial-temporal lobes is tightly linked to long-term memory (Halgren et al., 2015; Staresina, Fell, Do Lam, Axmacher, & Henson, 2012; Fell & Axmacher, 2011; Sederberg, Kahana, Howard, Donner, & Madsen, 2003; Fell et al., 2001). Our theta effects for semantic object properties in the pVTC and the ATL are consistent with intracranial recordings in humans from anterior IT and the PRC, which show a modulation of theta activity according to the semantic category of words (Halgren et al., 2015), where it is further hypothesized that ATL structures aid the encoding of attributes in coordination with theta in the hippocampus (Halgren et al., 2015; Staresina et al., 2012; Fell et al., 2001).

One novel hypothesis from our study is that different primary rhythms may encode visual and semantic properties in the ATL. The concept that different frequencies code complementary aspects of a stimulus is known as multiplexing. Using EEG, Schyns et al. (2011) showed that posterior electrodes coded for the eyes of a face in the beta band and the mouth in theta, showing that different features of a face are coded in different frequencies. In our study, different object features relating to vision and semantics peaked at different frequencies in the ATL—alpha and theta. Recently, the PRC within the ATL was shown to represent both high-level visual properties and conceptual properties of objects (Martin, Douglas, Newsome, Man, & Barense, 2018). Our evidence of visual and semantic effects in the ATL may indicate that the conjoint coding of visual and conceptual properties in the PRC could be aided through a multiplexed coding scheme, which may also be useful for integrating distinct visual information within a forming semantic representation. We can speculate that given that we find visual effects in low frequencies, peaking at alpha, the slower theta dynamics for semantics could

be useful to integrate semantic information from the environment over multiple alpha cycles. However, the currently study, while finding significant differences in the peak frequencies for visual and semantic models, would require additional support for this hypothesis. Further ECOG investigations will be important to highlight the specific spatiotemporal-spectral signatures for vision and semantics in the ATL and how complementary aspects of low-frequency activity relate to specific properties of objects. These studies would also offer the opportunity to test how low-frequency phase information and high-frequency activity (>100 Hz) might jointly represent object information through phase–amplitude coupling (Jensen et al., 2014; Canolty & Knight, 2010; Jensen & Mazaheri, 2010). This is supported by recent work showing that high-frequency activity to different object categories occurs at different phases of a low-frequency oscillation, showing how phase–amplitude coupling could relate to phase coding (Watrous, Deuker, et al., 2015).

One clear step forward provided by our study is determining how object information across different brain areas was related (also see Goddard, Carlson, Dermody, & Woolgar, 2016; Ince et al., 2015, for related approaches). This is an important step because, although our main analyses highlight parallel hierarchies of vision to semantics and posterior to anterior regions, this is likely an oversimplification of the underlying activity dynamics. By combining the RSA time courses with GC, we were able to show how information in one region changes the state of information in another region, characterizing how information flows in the VVP.

As predicted by most models of visual processing, our analysis showed visual object information was associated with feedforward connectivity, in that visual representations coded in occipital low-frequency phase predicted future visual representations in more anterior regions in the VVP. In contrast, the flow of semantic representation effects was feedback and cross-hemispheric, similar to previous reports of feedback activity in the VVP supporting semantic processing (Poch et al., 2015; Campo et al., 2013; Schendan & Ganis, 2012; Chan et al., 2011; Clarke et al., 2011). Crucially, this analysis enabled us to test the novel question of how visual representations impact future semantic representations. This analysis showed two prominent motifs: (1) visual effects in the occipital region related to subsequent semantic effects in the ATL and pVTC (feedforward) and (2) visual effects in the ATL related to subsequent semantic effects in the pVTC (feedback). This analysis revealed more complex dynamics than suggested when only looking at peak effects while also emphasizing the importance of the ATL through receiving feedforward inputs and sending top-down signals to posterior regions.

The ATL plays a central role in many theories of semantics, with differential emphasis of lateral, polar, and medial aspects of the region, which may depend on stimulus

modality or task (Mehta et al., 2016; Clarke & Tyler, 2015; Ralph, 2014; Patterson, Nestor, & Rogers, 2007; Damasio, Tranel, Grabowski, Adolphs, & Damasio, 2004; Grabowski et al., 2001). Given the spatial specificity of MEG source localization, we did not look to test between these positions and focus on the general role of the extended region. However, recent fMRI work using the same DNN and semantic AN approach shows that semantic effects for visual objects are represented in the PRC (Devereux et al., 2018), which is consistent with a variety of other neuroimaging and neuropsychology studies showing the semantics of visual objects is dependent on the PRC (Wright, Randall, Clarke, & Tyler, 2015; Clarke & Tyler, 2014; Tyler et al., 2013; Kivisaari et al., 2012; Taylor et al., 2006). Although we do not make claims about exact localization of ATL effects from this study, our results do provide critical new evidence of spectral and connectivity profiles that can further refine these accounts. One speculative prediction we can make regarding the ATL role is that it initially integrates visual signals during a feedforward alpha drive while activating semantic object properties. The properties, represented by theta activity, then communicated through feedback activity to the pVTC (Clarke, 2015; Chan et al., 2011), with coherent activity between the posterior and anterior regions in the VVP supporting the object-specific semantics (Clarke et al., 2011) based on top–down semantic and bottom–up visual signals. Theta activity may further structure alternating modes of feedforward and feedback activity (Halgren et al., 2015), with increased recurrent activity necessary under ambiguous perceptual conditions (Schendan & Ganis, 2012). Future studies utilizing ECOG or depth electrodes could begin to test these predictions.

Although research with time-sensitive approaches converge toward a model where the initial feedforward activation activates the visual aspects of objects before recurrent dynamics process the specific semantics (Clarke, 2015; Clarke & Tyler, 2015; Halgren et al., 2015; Poch et al., 2015; Schendan & Ganis, 2012; Chan et al., 2011), we lack an understanding of the neurocomputational principles of how vision activates meaning. Here, we tested whether oscillatory activity could represent stimulus-specific visual and semantic object properties and showed that visual properties were most associated with low-frequency phase and semantic properties were associated with theta phase information. Furthermore, distinct modes of connectivity underpinned the flow of information, where visual information flowed in a feedforward direction, semantics in feedback whereas the transfer between vision and semantics relied on feedforward, feedback, and intraregional flow. Our results highlight the ATL as an important region, both in representing visual and semantic information through a multiplexed code and for the transformation of information from visual to semantic. By combining oscillations, connectivity, RSA, and computational models, we show how visual signals activate meaning, taking us toward a more detailed model of object recognition.

Acknowledgments

This work was supported by a European Research Council Advanced Investigator grant under the European Community's Horizon 2020 Research and Innovation Programme (2014-2020 ERC grant agreement no. 669820) to L. K. T. and by the European Research Council under the European Community's Seventh Framework Programme (FP7/2007-2013)/ERC grant agreement no. 249640 to L. K. T.).

Reprint requests should be sent to Alex Clarke, Department of Psychology, University of Cambridge, Downing Street, Cambridge, CB2 3EB, United Kingdom, or via e-mail: ac584@cam.ac.uk.

REFERENCES

- Barense, M. D., Groen, I. I. A., Lee, A. C. H., Yeung, L., Brady, S. M., Gregori, M., et al. (2012). Intact memory for irrelevant information impairs perception in amnesia. *Neuron*, *75*, 157–167.
- Barnett, L., & Seth, A. K. (2014). The MVGC multivariate Granger causality toolbox: A new approach to Granger-causal inference. *Journal of Neuroscience Methods*, *223*, 50–68.
- Barrett, A. B., Murphy, M., Bruno, M.-A., Noirhomme, Q., Boly, M., Laureys, S., et al. (2012). Granger causality analysis of steady-state electroencephalographic signals during propofol-induced anaesthesia. *PLoS One*, *7*, e29072.
- Berens, P. (2009). CircStat: A MATLAB toolbox for circular statistics. *Journal of Statistical Software*, *31*. doi:10.18637/jss.v031.i10.
- Bullier, J. (2001). Integrated model of visual processing. *Brain Research Reviews*, *36*, 96–107.
- Bussey, T. J., & Saksida, L. M. (2002). The organization of visual object representations: A connectionist model of effects of lesions in perirhinal cortex. *European Journal of Neuroscience*, *15*, 355–364.
- Campo, P., Poch, C., Toledano, R., Igoa, J. M., Belinchon, M., Garcia-Morales, I., et al. (2013). Anterobasal temporal lobe lesions alter recurrent functional connectivity within the ventral pathway during naming. *Journal of Neuroscience*, *33*, 12679–12688.
- Canolty, R. T., & Knight, R. T. (2010). The functional role of cross-frequency coupling. *Trends in Cognitive Sciences*, *14*, 506–515.
- Chan, A. M., Baker, J. M., Eskandar, E., Schomer, D., Ulbert, I., Marinkovic, K., et al. (2011). First-pass selectivity for semantic categories in human anteroventral temporal cortex. *Journal of Neuroscience*, *31*, 18119–18129.
- Chaumon, M., Bishop, D. V. M., & Busch, N. A. (2015). A practical guide to the selection of independent components of the electroencephalogram for artifact correction. *Journal of Neuroscience Methods*, *250*, 47–63.
- Cichy, R. M., Khosla, A., Pantazis, D., Torralba, A., & Oliva, A. (2016). Comparison of deep neural networks to spatio-temporal cortical dynamics of human visual object recognition reveals hierarchical correspondence. *Scientific Reports*, *6*, 27755.
- Cichy, R. M., Pantazis, D., & Oliva, A. (2014). Resolving human object recognition in space and time. *Nature Neuroscience*, *17*, 455–462.
- Clarke, A. (2015). Dynamic information processing states revealed through neurocognitive models of object semantics. *Language, Cognition and Neuroscience*, *30*, 409–419.
- Clarke, A., Devereux, B. J., Randall, B., & Tyler, L. K. (2015). Predicting the time course of individual objects with MEG. *Cerebral Cortex*, *25*, 3602–3612.
- Clarke, A., Taylor, K. I., Devereux, B., Randall, B., & Tyler, L. K. (2013). From perception to conception: How meaningful objects are processed over time. *Cerebral Cortex*, *23*, 187–197.
- Clarke, A., Taylor, K. I., & Tyler, L. K. (2011). The evolution of meaning: Spatiotemporal dynamics of visual object recognition. *Journal of Cognitive Neuroscience*, *23*, 1887–1899.
- Clarke, A., & Tyler, L. K. (2014). Object-specific semantic coding in human perirhinal cortex. *Journal of Neuroscience*, *34*, 4766–4775.
- Clarke, A., & Tyler, L. K. (2015). Understanding what we see: How we derive meaning from vision. *Trends in Cognitive Sciences*, *19*, 677–687.
- Cowell, R. A., Bussey, T. J., & Saksida, L. M. (2010). Components of recognition memory: Dissociable cognitive processes or just differences in representational complexity? *Hippocampus*, *20*, 1245–1262.
- Cree, G. S., McNorgan, C., & McRae, K. (2006). Distinctive features hold a privileged status in the computation of word meaning: Implications for theories of semantic memory. *Journal of Experimental Psychology: Learning, Memory, and Cognition*, *32*, 643–658.
- Cree, G. S., & McRae, K. (2003). Analyzing the factors underlying the structure and computation of the meaning of chipmunk, cherry, chisel, cheese, and cello (and many other such concrete nouns). *Journal of Experimental Psychology: General*, *132*, 163–201.
- Cree, G. S., McRae, K., & McNorgan, C. (1999). An attractor model of lexical conceptual processing: Simulating semantic priming. *Cognitive Science*, *23*, 371–414.
- Crivelli-Decker, J., Hsieh, L.-T., Clarke, A., & Ranganath, C. (2018). Theta oscillations promote temporal sequence learning. *Neurobiology of Learning and Memory*, *153*, 92–103.
- Damasio, H., Tranel, D., Grabowski, T., Adolphs, R., & Damasio, A. (2004). Neural systems behind word and concept retrieval. *Cognition*, *92*, 179–229.
- Delorme, A., & Makeig, S. (2004). EEGLAB: An open source toolbox for analysis of single-trial EEG dynamics including independent component analysis. *Journal of Neuroscience Methods*, *134*, 9–21.
- Devereux, B. J., Clarke, A., & Tyler, L. K. (2018). Integrated deep visual and semantic attractor neural network models predict fMRI pattern-information across the ventral object processing pathway. *Scientific Reports*, *8*, article 10636.
- Devereux, B. J., Taylor, K. I., Randall, B., Geertzen, J., & Tyler, L. K. (2016). Feature statistics modulate the activation of meaning during spoken word processing. *Cognitive Science*, *40*, 325–350.
- Devereux, B. J., Tyler, L. K., Geertzen, J., & Randall, B. (2014). The Centre for Speech, Language and the Brain (CSLB) concept property norms. *Behavior Research Methods*, *46*, 1119–1127.
- DiCarlo, J. J., Zoccolan, D., & Rust, N. C. (2012). How does the brain solve visual object recognition? *Neuron*, *73*, 415–434.
- Fell, J., & Axmacher, N. (2011). The role of phase synchronization in memory processes. *Nature Reviews Neuroscience*, *12*, 105–118.
- Fell, J., Klaver, P., Lehnertz, K., Grunwald, T., Schaller, C., Elger, C. E., et al. (2001). Human memory formation is accompanied by rhinal-hippocampal coupling and decoupling. *Nature Neuroscience*, *4*, 1259.
- Goddard, E., Carlson, T. A., Dermody, N., & Woolgar, A. (2016). Representational dynamics of object recognition: Feedforward and feedback information flows. *Neuroimage*, *128*, 385–397.
- Grabowski, T. J., Damasio, A. R., Tranel, D., Pronto, L. L., Hichwa, R. D., & Damasio, A. R. (2001). A role for left temporal pole in the retrieval of words for unique entities. *Human Brain Mapping*, *13*, 199–212.
- Güçlü, U., & van Gerven, M. A. J. (2015). Deep neural networks reveal a gradient in the complexity of neural representations

- across the ventral stream. *Journal of Neuroscience*, 35, 10005–10014.
- Halgren, E., Kaestner, E., Marinkovic, K., Cash, S. S., Wang, C., Schomer, D. L., et al. (2015). Laminar profile of spontaneous and evoked theta: Rhythmic modulation of cortical processing during word integration. *Neuropsychologia*, 76, 108–124.
- Hanslmayr, S., Staudigl, T., & Fellner, M.-C. (2012). Oscillatory power decreases and long-term memory: The information via desynchronization hypothesis. *Frontiers in Human Neuroscience*, 6, 74.
- Helfrich, R. F., & Knight, R. T. (2016). Oscillatory dynamics of prefrontal cognitive control. *Trends in Cognitive Sciences*, 20, 916–930.
- Hipp, J. F., & Siegel, M. (2015). Accounting for linear transformations of EEG and MEG data in source analysis. *PLoS One*, 10, e0121048.
- Ince, R. A. A., van Rijsbergen, N. J., Thut, G., Rousselet, G. A., Gross, J., Panzeri, S., et al. (2015). Tracing the flow of perceptual features in an algorithmic brain network. *Scientific Reports*, 5, 17681.
- Jensen, O., Gips, B., Bergmann, T. O., & Bonnefond, M. (2014). Temporal coding organized by coupled alpha and gamma oscillations prioritize visual processing. *Trends in Neurosciences*, 37, 357–369.
- Jensen, O., & Mazaheri, A. (2010). Shaping functional architecture by oscillatory alpha activity: Gating by inhibition. *Frontiers in Human Neuroscience*, 4, 186.
- Jia, Y., Shelhamer, E., Donahue, J., Karayev, S., Long, J., Girshick, R., et al. (2014). Caffe: Convolutional architecture for fast feature embedding. ArXiv14085093 Cs.
- Kayser, C., Ince, R. A. A., & Panzeri, S. (2012). Analysis of slow (theta) oscillations as a potential temporal reference frame for information coding in sensory cortices. *PLoS Computational Biology*, 8, e1002717.
- Kivisaari, S. L., Tyler, L. K., Monsch, A. U., & Taylor, K. I. (2012). Medial perirhinal cortex disambiguates confusable objects. *Brain*, 135, 3757–3769.
- Klimesch, W., Sauseng, P., & Hanslmayr, S. (2007). EEG alpha oscillations: The inhibition–timing hypothesis. *Brain Research Reviews*, 53, 63–88.
- Kravitz, D. J., Saleem, K. S., Baker, C. I., Ungerleider, L. G., & Mishkin, M. (2013). The ventral visual pathway: An expanded neural framework for the processing of object quality. *Trends in Cognitive Sciences*, 17, 26–49.
- Kriegeskorte, N., Mur, M., & Bandettini, P. (2008). Representational similarity analysis—Connecting the branches of systems neuroscience. *Frontiers in Systems Neuroscience*, 2, 4.
- Krizhevsky, A., Sutskever, I., & Hinton, G. E. (2012). ImageNet classification with deep convolutional neural networks. In *Advances in neural information processing* (pp. 1097–1105). Cambridge, MA: MIT Press.
- Lamme, V., & Roelfsema, P. (2000). The distinct modes of vision offered by feedforward and recurrent processing. *Trends in Neurosciences*, 23, 571–579.
- Lisman, J. E., & Jensen, O. (2013). The theta-gamma neural code. *Neuron*, 77, 1002–1016.
- Lopour, B. A., Tavassoli, A., Fried, I., & Ringach, D. L. (2013). Coding of information in the phase of local field potentials within human medial temporal lobe. *Neuron*, 79, 594–606.
- Maris, E., & Oostenveld, R. (2007). Nonparametric statistical testing of EEG- and MEG data. *Journal of Neuroscience Methods*, 164, 177–190.
- Martin, C. B., Douglas, D., Newsome, R. N., Man, L. L., & Barense, M. D. (2018). Integrative and distinctive coding of visual and conceptual object features in the ventral visual stream. *eLife*, 7, e31873.
- Medvedovsky, M., Taulu, S., Bikmullina, R., Ahonen, A., & Paetau, R. (2009). Fine tuning the correlation limit of spatio-temporal signal space separation for magnetoencephalography. *Journal of Neuroscience Methods*, 177, 203–211.
- Mehta, S., Inoue, K., Rudrauf, D., Damasio, H., Tranel, D., & Grabowski, T. (2016). Segregation of anterior temporal regions critical for retrieving names of unique and non-unique entities reflects underlying long-range connectivity. *Cortex*, 75, 1–19.
- Michelmann, S., Bowman, H., & Hanslmayr, S. (2016). The temporal signature of memories: Identification of a general mechanism for dynamic memory replay in humans. *PLoS Biology*, 14, e1002528.
- Mollo, G., Cornelissen, P. L., Millman, R. E., Ellis, A. W., & Jefferies, E. (2017). Oscillatory dynamics supporting semantic cognition: MEG evidence for the contribution of the anterior temporal lobe hub and modality-specific spokes. *PLoS One*, 12, e0169269.
- Montemurro, M. A., Rasch, M. J., Murayama, Y., Logothetis, N. K., & Panzeri, S. (2008). Phase-of-firing coding of natural visual stimuli in primary visual cortex. *Current Biology*, 18, 375–380.
- Ng, B. S. W., Logothetis, N. K., & Kayser, C. (2013). EEG phase patterns reflect the selectivity of neural firing. *Cerebral Cortex*, 23, 389–398.
- Nichols, T. E., & Holmes, A. P. (2002). Nonparametric permutation tests for functional neuroimaging: A primer with examples. *Human Brain Mapping*, 15, 1–25.
- Nili, H., Wingfield, C., Walther, A., Su, L., Marslen-Wilson, W., & Kriegeskorte, N. (2014). A toolbox for representational similarity analysis. *PLoS Computational Biology*, 10, e1003553.
- Panzeri, S., Macke, J. H., Gross, J., & Kayser, C. (2015). Neural population coding: Combining insights from microscopic and mass signals. *Trends in Cognitive Sciences*, 19, 162–172.
- Patterson, K., Nestor, P. J., & Rogers, T. T. (2007). Where do you know what you know? The representation of semantic knowledge in the human brain. *Nature Reviews Neuroscience*, 8, 976–988.
- Poch, C., Garrido, M. I., Igoa, J. M., Belinchón, M., García-Morales, I., & Campo, P. (2015). Time-varying effective connectivity during visual object naming as a function of semantic demands. *Journal of Neuroscience*, 35, 8768–8776.
- Ralph, M. A. L. (2014). Neurocognitive insights on conceptual knowledge and its breakdown. *Philosophical Transactions of the Royal Society of London, Series B, Biological Sciences*, 369, 20120392.
- Randall, B., Moss, H. E., Rodd, J. M., Greer, M., & Tyler, L. K. (2004). Distinctiveness and correlation in conceptual structure: Behavioral and computational studies. *Journal of Experimental Psychology: Learning, Memory, and Cognition*, 30, 393–406.
- Rogers, T. T., & McClelland, J. L. (2004). *Semantic cognition: A parallel distributed approach*. Cambridge, MA: MIT Press.
- Schendan, H. E., & Ganis, G. (2012). Electrophysiological potentials reveal cortical mechanisms for mental imagery, mental simulation, and grounded (embodied) cognition. *Frontiers in Psychology*, 3, 329.
- Schendan, H. E., & Maher, S. M. (2009). Object knowledge during entry-level categorization is activated and modified by implicit memory after 200 ms. *Neuroimage*, 44, 1423–1438.
- Schyns, P. G., Thut, G., & Gross, J. (2011). Cracking the code of oscillatory activity. *PLoS Biology*, 9, e1001064.
- Sederberg, P. B., Kahana, M. J., Howard, M. W., Donner, E. J., & Madsen, J. R. (2003). Theta and gamma oscillations during encoding predict subsequent recall. *Journal of Neuroscience*, 23, 10809–10814.
- Seeliger, K., Fritsche, M., Güçlü, U., Schoenmakers, S., Schoffelen, J.-M., Bosch, S. E., et al. (2017). Convolutional neural network-based encoding and decoding of visual object recognition in space and time. *Neuroimage*. doi:10.1016/j.neuroimage.2017.07.018.

- Staresina, B. P., Fell, J., Do Lam, A. T. A., Axmacher, N., & Henson, R. N. (2012). Memory signals are temporally dissociated in and across human hippocampus and perirhinal cortex. *Nature Neuroscience*, *15*, 1167–1173.
- Staudigl, T., Vollmar, C., Noachtar, S., & Hanslmayr, S. (2015). Temporal-pattern similarity analysis reveals the beneficial and detrimental effects of context reinstatement on human memory. *Journal of Neuroscience*, *35*, 5373–5384.
- Supp, G., Schlogl, A., Trujillo-Barreto, N., Müller, M. M., & Gruber, T. (2007). Directed cortical information flow during human object recognition: Analyzing induced EEG gamma-band responses in brain's source space. *PLoS One*, *2*, 1–11.
- Tallon-Baudry, C., & Bertrand, O. (1999). Oscillatory gamma activity in humans and its role in object representation. *Trends in Cognitive Sciences*, *3*, 151–162.
- Taylor, K. I., Devereux, B. J., & Tyler, L. K. (2011). Conceptual structure: Towards an integrated neurocognitive account. *Language and Cognitive Processes*, *26*, 1368–1401.
- Taylor, K. I., Moss, H. E., Stamatakis, E. A., & Tyler, L. K. (2006). Binding crossmodal object features in perirhinal cortex. *Proceedings of the National Academy of Sciences, U.S.A.*, *103*, 8239–8244.
- Turesson, H. K., Logothetis, N. K., & Hoffman, K. L. (2012). Category-selective phase coding in the superior temporal sulcus. *Proceedings of the National Academy of Sciences, U.S.A.*, *109*, 19438–19443.
- Tyler, L. K., Chiu, S., Zhuang, J., Randall, B., Devereux, B. J., Wright, P., et al. (2013). Objects and categories: Feature statistics and object processing in the ventral stream. *Journal of Cognitive Neuroscience*, *25*, 1723–1735.
- Tyler, L. K., & Moss, H. E. (2001). Towards a distributed account of conceptual knowledge. *Trends in Cognitive Sciences*, *5*, 244–252.
- Tyler, L. K., Stamatakis, E. A., Bright, P., Acres, K., Abdallah, S., Rodd, J. M., et al. (2004). Processing objects at different levels of specificity. *Journal of Cognitive Neuroscience*, *16*, 351–362.
- VanRullen, R., Zoefel, B., & Ilhan, B. (2014). On the cyclic nature of perception in vision versus audition. *Philosophical Transactions of the Royal Society of London, Series B, Biological Sciences*, *369*, 20130214.
- Watrous, A. J., Deuker, L., Fell, J., & Axmacher, N. (2015). Phase-amplitude coupling supports phase coding in human ECoG. *eLife*, *4*, e07886.
- Watrous, A. J., Fell, J., Ekstrom, A. D., & Axmacher, N. (2015). More than spikes: Common oscillatory mechanisms for content specific neural representations during perception and memory. *Current Opinion in Neurobiology*, *31*, 33–39.
- Wright, P., Randall, B., Clarke, A., & Tyler, L. K. (2015). The perirhinal cortex and conceptual processing: Effects of feature-based statistics following damage to the anterior temporal lobes. *Neuropsychologia*, *76*, 192–207.
- Zeiler, M. D., & Fergus, R. (2014). Visualizing and understanding convolutional networks. In *Computer vision—ECCV 2014* (pp. 818–833). Cham: Springer.
- Zumer, J. M., Scheeringa, R., Schoffelen, J.-M., Norris, D. G., & Jensen, O. (2014). Occipital alpha activity during stimulus processing gates the information flow to object-selective cortex. *PLoS Biology*, *12*, e1001965.